Remote Sensing of Environment 133 (2013) 183–192

Contents lists available at SciVerse ScienceDirect

Remote Sensing of Environment

journal homepage: www.elsevier.com/locate/rse

# Dynamic response of microwave land surface properties to precipitation in Amazon rainforest

Rui Li, Qilong Min *

*Atmospheric Science Research Center, State University of New York, Albany NY 12203, USA*

ARTICLE INFO

*Article history:*
Received 8 November 2012
Received in revised form 31 January 2013
Accepted 3 February 2013
Available online 17 March 2013

*Keywords:*
Microwave land surface emissivity
Soil moisture
Vegetation
Precipitation

ABSTRACT

The responses of land surface microwave properties to precipitation, including the brightness temperature (Tbs) and emissivities (MLSEs) at 18.7, 23.8 and 37.0 GHz, are studied by combining satellite synergetic retrievals (from AQUA AMSR-E and MODIS) with in-situ measured land surface temperature, soil moisture (SM), and precipitation at two Amazonia tropical rainforest sites Km83 and Km67. In general, Tbs and MLSEs are found to be negatively correlated to SM. Their dependences on the vegetation water content (VWC) are not monotonic: positive correlations at relatively low VWC and negative correlations at high VWC range. Although Amazon dense rainforest is the most stable vegetation regime, there are significant seasonal variations in both MLSE and Tbs, with amplitudes of about 0.025 and 7.0 K, respectively. The day-to-day variation of MLSE and Tbs is larger in the wet seasons than in the dry seasons, although the mean MLSE and Tbs are lower in the wet seasons than in the dry seasons. After precipitation, the SM, VWC and canopy interception water increase and reach their peak values at different transit times. There is an equilibrium time point (about 4 h in this case) at which the vegetation–soil system holds the largest amount of moisture. Consequently, Tbs and MLSEs decrease during the first several hours after the start of precipitation and then increase after the equilibrium time point. Ignoring the "turning point" may introduce significant errors in the estimation of MLSEs (up to 0.04) and Tbs (up to 10 K) under rainy conditions.



## 1. Introduction

The land surface plays key roles in the water, carbon, and energy cycles in the Earth climate system at a variety of time and spatial scales, by receiving impacts from and regulating feedbacks to the atmosphere. Such interactions are especially strong in dense vegetation covered areas such as the Amazon tropical rainforest. The broad spectra of spatial and temporal scales of climate system and inherent heterogeneity of the biosphere require the use of satellite remote sensing techniques to study and monitor surface/soil/canopy states and the related atmospheric and environmental processes. In particular, the soil moisture (SM) and vegetation water content (VWC) are the two most important parameters controlling the physical and phenological processes of the land surface. Precipitation makes direct impacts on soil moisture and canopy water through infiltration and interception. Therefore, accurate measurements of SM, VWC, and precipitation overland are critical in understanding the climate system. However, optical sensors on satellite platform have their limitations in remotely sensing those parameters. Attention is paid to microwave sensors that are capable of measuring radiation emitted from the soil–vegetation–atmosphere medium. Remotely sensing SM, VWC, and precipitation from microwave sensors requires better understanding and qualifying of microwave land surface radiative properties under all-weather conditions, particularly under rainy conditions.

The upwelling microwave radiance at the top of atmosphere (TOA) has different sensitivities to different portions of the soil–vegetation–atmosphere medium, depending on its frequency. Microwave signals at low frequencies (e.g. 1.6 and 6.9 GHz, etc.) are more favorable to sense the land surface parameters due to their relative insensitivity to the atmosphere and their capability of deep soil penetration (Njoku, 1999 and reference therein). However, few existing rainfall algorithms include these low frequencies. Also, their spatial resolutions are significantly lower than the medium and higher frequencies. The microwave signals at high frequencies (85 GHz and higher) carry information of the land surface under clear-sky conditions, but they are severely affected by atmospheric hydrometeors under cloudy conditions (Grody, 1991; Liu et al., 1994; Spencer et al., 1989). Microwave signals at moderate frequencies, such as 18.7, 23.8 and 36.5 (hereafter 19, 24 and 37 for brief) GHz, are sensitive to both land surface and atmospheric properties (Aires et al., 2005; Morland et al., 2000, 2001; Lin & Minnis, 2000; Min & Lin, 2006a, 2006b; Prigent et al., 2005). Such a capability of moderate frequency microwave signals has been receiving increasing attention recently because of their potential applications in retrieving rainfall over land (Ferraro et al., 2013). We will focus on the microwave signals at 19, 24, and 37 GHz in this paper, to understand microwave land surface radiative properties, at those frequencies, under all weather conditions.

* Corresponding author. Tel.: +1 518 437 8742.
*E-mail address:* qmin@albany.edu (Q. Min).

0034-4257/$ – see front matter © 2013 Elsevier Inc. All rights reserved.
http://dx.doi.org/10.1016/j.rse.2013.02.001

It is well known that the microwave emissivity (reflectivity) of bare soil decreases (increases) with soil moisture because of the greater dielectric constant of water compared to other natural materials in the dry soil. Numerous studies using different data sources in different regions showed that the satellite retrieved microwave land surface emissivities (MLSEs) at multiple frequencies are negatively correlated to the soil moisture (Ulaby et al., 1986 and associated reference therein; Aires et al., 2005; Morland et al., 2000, 2001; Lin & Minnis, 2000; Norouzi et al., 2001; Prigent et al., 2005). However, there were some exceptions where the correlations could be either insignificant or even positive, mainly due to the complex inherent correlations between soil moisture and vegetation (e.g. Prigent et al., 2005). On the other hand, MLSEs are found, in general, increasing with vegetation mainly based on visible and infrared vegetation indexes (Morland et al., 2000, 2001; Norouzi et al., 2001; Prigent et al., 2005; Ruston & Vonder Haar, 2004). However, Min and Lin (2006a, Figure 2) pointed out that the relationship between MLSE and vegetation water content may be more complicate and not monotonic. With the aid of a simplified radiation transfer model in the soil–vegetation medium, they predicted that the MLSE increases with VWC due to the scattering and emission effects of the crown layer when VWC is relatively small. However, when VWC in the crown layer is large enough, the strong absorption of the crown attenuates the soil emission, resulting in the apparent emissivity dominated by the vegetation emissivity and decreased with VWC.

Clearly, MLSE is not static but a resultant of dynamical processes coupled land surface (soil and vegetation, snow pack in some regions) and the atmosphere, as both soil moisture and vegetation water content response to weather and climate changes. Clouds and associated boundary layer humidity enhance both radiation use efficiency and water use efficiency of forests (Min, 2005), and consequently lead to changes in the canopy VWC and SM. Rain events more directly change soil moisture and canopy water (internal vegetation water content and/or intercepted water on leaves), resulting in changes in MLSE. The net effect on MLSE is very complicated and is strongly dependent upon the soil and vegetation properties, as well as cloud and precipitation properties (amount, during, intensity, and type). Morland et al., (2000, 2001) reported that there was a positive correlation between MLSE and Normalized Difference Vegetation Index (NDVI) over dry land surface, but such a correlation became weak under wet land surface conditions (after rain events). Ferraro et al. (2013) also found MLSE dropped after significant rainfall and the changes were dependent on how dry the soil was before the rain event. Most MLSEs used in previous studies were retrieved under clear-sky conditions due to the increasing uncertainties introduced by cloud hydrometeors in the radiation transfer process. There is no systematic study of MLSE changes in the transition from clear-sky to cloudy and to rainy conditions. By using the synergized satellite retrievals of cloud and the microwave brightness temperature, we developed an algorithm to retrieve MLSE under both clear and non-rainy cloudy conditions (Min & Lin, 2006a; Min et al., 2010). In this study, we combine the non-rainy all weather retrievals with the in-situ measurements at two Amazon sites to investigate the dynamic response of land surface microwave properties to SM, VWC and precipitation.

## 2. Data and methodology

### 2.1. In-situ measurements

The in-situ measurements used in this study were collected from two Amazon primary tropical rainforest sites: the Km83 (3°03′S, 54°56′W, from 2002 Jul to 2004 Jan) and Km67 (2°51′S, 54°58′W, from 2002 Jul to 2006 Jan), shown in Fig. 1, operated as part of the Large-scale Biosphere–Atmosphere Experiment in Amazonia (Hutyra et al., 2007; Miller et al., 2009; Saleska et al., 2003). The vegetation around the Km83 site was tropical humid forest on a flat plateau, with a canopy height of 20–40 m. The Km67 site was in an old-growth forest with a canopy height up to 43 m. The mean annual precipitation was about 1920 mm at the site. The precipitation was measured at 64 m height every 30 min at the Km83 site and at 42.6 m height every 1.0 h at the Km67 site. These measurements actually represent the precipitation at the top of the canopy not at the surface. For some very weak precipitation, the rain water may not fall through the canopy due to the interception. However, there was no direct measurement of canopy intercepted water. Using eddy-covariance data, Czikowsky and Fitzjarrald (2009) estimated that the mean interception for moderate daytime rainfall-rate events was about 10% at the Km67 site, with light events at 18% and heavy events at 7.8%.

The soil moisture was measured at 10, 20 and 40 cm depth every 30 min at the Km83 site but not available at the Km67 site. Considering the penetration depth (the order of 0.1–1 cm) of the microwave radiance at the frequencies of 19, 24 and 37 GHz, the 10 cm SM might be significantly different from the effective soil moisture that influences the microwave radiance. However, using the 10 cm measurements is the best way we can do to represent the near surface soil moisture. For the Km67 site, where SM measurements were not available, we use the dry duration (DD) as an indicator of soil moisture or the soil potential wetness. DD is estimated from the high temporal resolution in-situ precipitation records as the time duration between a given time point to the latest rain event. The underlying assumption is that no rain event was missed by the in-situ measurements. Since satellite retrievals of MLSE cannot be obtained during a rain event, the dependence of MLSE on DD (always larger than zero) may provide a bridge to extrapolate the non-rainy MLSE behavior to the rainy MLSE. In addition, the air temperatures measured at multiple heights from 2 m to 64 m were used to derive the needed land surface temperature for the satellite retrievals.

### 2.2. Satellite retrievals

A key step for understanding the sensitivity of land surface microwave properties to environmental parameters is to obtain all non-rainy weather retrievals, particularly under cloudy conditions. We

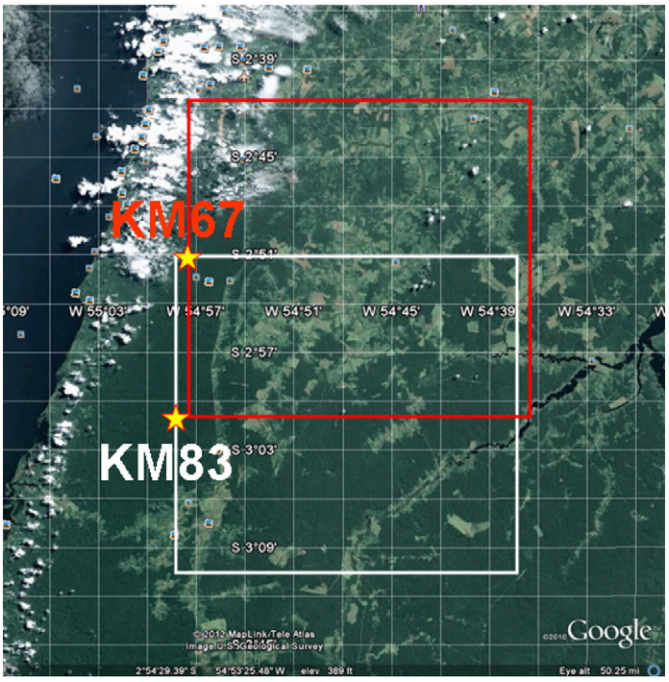


**Fig. 1.** The locations and terrestrial features of the two sites of Km83 and Km67 in the snapshot of Google Earth and the selected areas for collocating with satellite observations.

have developed this required algorithm by combining microwave measurements with visible and infrared observations (Li et al., 2009; Lin & Minnis, 2000; Min & Lin, 2006a, 2006b; Min et al., 2010). This synergetic retrieval algorithm, with careful treatments of horizontal inhomogeneity of cloud fields, cloud vertical distribution and cloud phase partition, allows us to get retrievals of MLSE under both clear-sky and cloudy conditions. We use Aqua Advanced Microwave Scanning Radiometer for EOS (AMSR-E) measured multiple channels of microwave brightness temperature at TOA as the primary input. The MODerate resolution Imaging Spectroradiometer (MODIS) on Aqua provides the visible and infrared measurements of aerosol and cloud fields (1 km resolution) within the relatively large field of view (FOV) of AMSR-E. To deal with the sub-FOV horizontal inhomogeneity, a Gaussian weighting function of each individual MODIS pixel within the AMSR-E FOV is applied. The retrievals from different channels and polarizations are made using an atmospheric microwave radiative transfer (MWRT) model with information of clouds, water vapor, other atmospheric gases, and land surface temperature (LST). The MWRT model accounts for the atmospheric absorption and emission of gases and clouds, especially the temperature and pressure dependences of these radiative properties (Lin et al., 1998, 2001). The detailed method for integrating satellite microwave measurements with visible and infrared observations and reanalysis dataset to retrieve MLSE has been described in Min and Lin (2006a) and Min et al. (2010).

The uncertainty in LST is known as one of the greatest error sources for the MLSE retrievals (Ferraro et al., 2013; Jiménez et al., 2012; Yang & Weng, 2011; Zheng et al., 2012). Due to the different penetration depth at different frequencies, LST is actually frequency-dependent. In this study, the in-situ measured air temperatures at 2 m and 64 m heights at 1:30 PM each day are used to estimate LST, following the empirical relationship between LST and near surface air temperature based on NCEP reanalysis data. Although we try our best to minimize the uncertainty of LST in MLSE retrievals, some errors or biases exist. To further avoid such an uncertainty, we also investigate the sensitivity of the microwave brightness temperature at the land surface (Tbs). Tbs is not affected by the uncertainty of LST estimation and shows more consistency among different algorithms (Ferraro et al., 2013).

Existing satellite remote sensing for vegetation detection is based on spectral measurements at visible and near-infrared wavelengths that are correlated to the absorbed fraction of photosynthetically active radiation (PAR), such as normalized difference vegetation index (NDVI), and enhanced vegetation index (EVI). These vegetation indexes, however, are highly sensitive to clouds and aerosols (unable to provide information under cloudy conditions) and saturate at intermediate values of leaf area index (LAI) (Asrar et al., 1984; Granger, 2000; Gutman, 1999; Min et al., 2010; Myneni et al., 1995; Sellers, 1985). To alleviate this problem in the dense vegetation regions with high cloud covers, i.e., Amazon basin, we utilize the microwave based vegetation index proposed by Min and Lin (2006a), i.e., microwave Emissivity Difference Vegetation Index (EDVI) in this study. The EDVI is defined as the MLSE differences between 19 GHz and 37 GHz, i.e. $EDVI = 2(MLSE_{19} - MLSE_{37})/(MLSE_{19} + MLSE_{37})$.

The microwave surface emission above a canopy is an integration of the microwave radiation from the whole canopy vertical profile and the soil weighted by its transmission. The emissivity observed at longer wavelengths with a weaker attenuation by the canopy generally represents an effectively thicker layer than those observed at shorter and stronger attenuation wavelengths. EDVI can provide a measure of VWC (and remaining canopy intercepted water) with a minimal influence of the soil emission underneath vegetation canopy (Li et al., 2009; Min & Lin, 2006a, 2006b; Min et al., 2010).

### 2.3. Collocations between in-situ measurements and the satellite retrievals

Since the two sites are close to the Amazon River, we carefully select two domains (0.36°×0.36°) around these sites to avoid contaminations from the river, illustrated in Fig. 1. The Aqua overpasses the select domains at about 1:30 pm local time (LT). In each overpass, Tbs, MLSE, and EDVI are retrieved for all non-rainy AMSR-E FOVs within the two selected domains. LST for AMSR-E FOV is assumed to be the same as that estimated at the Km83 and Km67 sites. Then all of the retrievals are averaged over the 0.36°×0.36° domain to represent the mean Tbs, MLSE and EDVI at these sites to minimize the potential sub-FOV spatial variability (agriculture patches and uncovered bare soil spots). Finally, the averaged Tbs, MLSE and EDVI are collocated with the in-situ measurements of SM, DD, and precipitation.

## 3. Results

MLSE is determined by the dielectric constant of the dry soil, the soil moisture (SM), the surface roughness, the structure of vegetation, the vegetation water content (VWC) and the canopy interception water. The SM, VWC and canopy interception water change rapidly through the dynamical processes coupled land surface and the atmosphere at inter-annul, seasonal and diurnal scales. To understand physical mechanisms of the MLSE dynamics, we first look into the time series of satellite retrieved Tbs, MLSE and EDVI (retrievals are available only under non-rainy conditions) with the associated in-situ measurements of SM and precipitation, as shown in Figs. 2 and 3. At both sites, soil and vegetation experienced distinct dry (July to November) and wet (December to June) seasons. SM abruptly increased when precipitation occurred and decreased slowly and exponentially in the dry period as a result of evaporation (Fig. 2). As expected, the mean level of SM was relatively lower in the dry season than in the wet season. EDVI, as an indicator of VWC and interception water, decreased with the dry duration and reached its minimum in the middle of dry seasons. Then it started to increase before the start of the wet season. The SM was relatively low and stable in the dry season. Although SM remained high with a slight increasing trend in the middle of the wet seasons, EDVI reached its peak earlier than SM and gradually decreased until another seasonal cycle. The phase of EDVI seasonality seemed to be in advance of the precipitation seasonal phase, suggesting a possible coupling mechanism in which evapotranspiration (which is positively correlated with EDVI, see Li et al. (2009)) from vegetation may trigger the wet season and enhance precipitation. The MLSE of vertical polarization at 19 GHz was higher in the dry season than in the wet season, with a seasonal mean difference of 0.025. Although the running averaged MLSE (red curve) tended to be more stable in the wet season than in the dry season, there were large day-to-day variations (up to 0.03) in the emissivity and this variation was mainly associated with precipitation and associated interception water. In the dry season with a long period of no-rain, there was an anti-correlation between MLSE and EDVI. As clearly shown in the period of Sept–Dec of 2002, where the baseline of SM was low and relatively constant, MLSE decreased with EDVI (or VWC), suggesting the positive impacts of VWC on MLSE. In the wet season, on the other hand, the relationships among SM, VWC and MLSE are more complicated and detailed investigations will be discussed below. In general, MLSEs at other frequencies and polarizations, not shown, have similar seasonality patterns of MLSE at 19 GHz. Tbs at 19 GHz varied from 286.2 to 293.4 K, shown in Fig. 2b, with seasonality similar to that of MLSE. Tbs at 37 GHz was about 3.4° lower than Tbs at 19 GHz due to the scattering depression from the vegetation elements (leaves, stems and branches, etc).

The results at the Km67 site are consistent with those at the Km83, shown in Fig. 3, except for the replacement of DD for the in-situ measured SM. DD has high values in the dry season and low values in the wet season (the DD is plotted in a reversed order in Fig. 3a). VWC as indicated by EDVI is strongly anti-correlated with *Log(DD)* at seasonal scales. The phase of VWC seasonality was slightly ahead those of *Log*(DD) and precipitation, consistent with the finding at the Km83

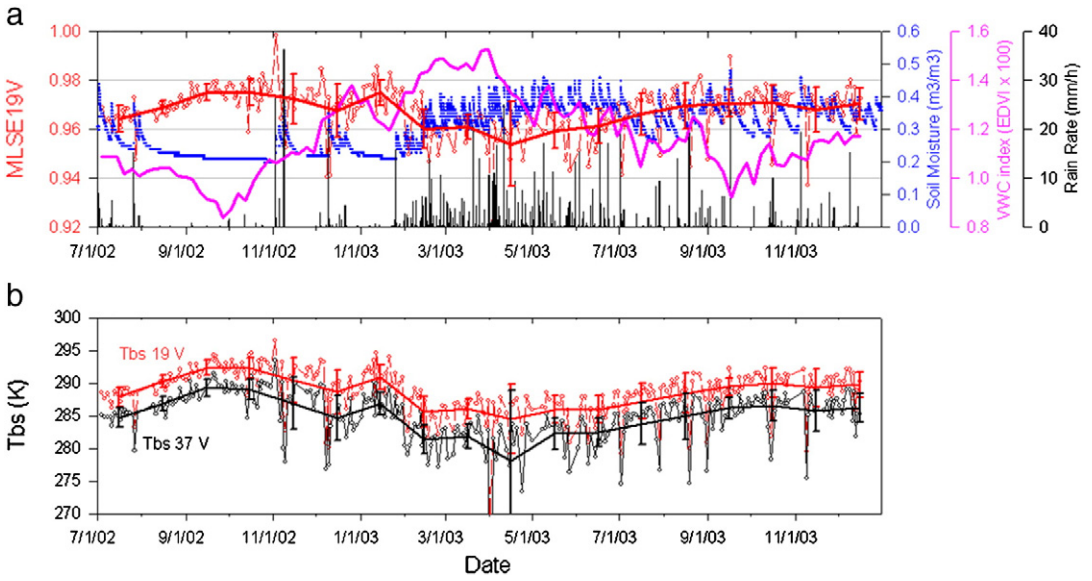


**Fig. 2.** Time series of (a) MLSE at 19 GHz (V polarization), soil moisture, EDVI the vegetation water content index and rain rate; (b) 19 and 37 GHz brightness temperatures (V polarization) at Km83 site.

site. MLSEs (and TBs) are also correlated with VWC (negative) and DD (positive) at seasonal scale.

### 3.1. Soil moisture

To understand the impact of soil–vegetation interaction on the microwave land surface brightness temperature and emissivity, we use a simple two-layer model and assume 1) the soil surface is uniform; 2) the vegetation layer has small single scattering albedo; and 3) the reflection at the vegetation–air interface can be ignored. Therefore the microwave brightness temperature $T_b$ at the top of the canopy can be expressed as:

$$T_b = T_s\varepsilon_s e^{-\tau/\mu} + T_c\left(1-e^{-\tau/\mu}\right)(1-\omega) + T_c\left(1-e^{-\tau/\mu}\right)(1-\omega)(1-\varepsilon_s)e^{-\tau/\mu} \quad (1)$$

where $T_s$, $T_c$, $\varepsilon_s$, $\omega$, $\tau$ and $\mu$ are the soil temperature, the canopy temperatures, the soil emissivity, the canopy single scattering albedo, the optical depth of the canopy, and the radiation direction, respectively. The first term of the right hand of Eq. (1) stands for the emission from the soil with the vegetation attenuation. The second term stands for the upwelling emission directly from the vegetation. The third term stands for the vegetation downwelling emission that is reflected by the soil and further attenuated by the vegetation.

Given the facts that $1-\varepsilon_s$ is one order of magnitude smaller than one and $e^{-\tau/\mu}$ is also smaller than one, we further ignore the third term:

$$T_b = T_s\varepsilon_s e^{-\tau/\mu} + T_c\left(1-e^{-\tau/\mu}\right)(1-\omega). \quad (2)$$

Further assuming the temperature difference between the soil and the vegetation is small (i.e. $T_s \approx T_c$); we will have the apparent

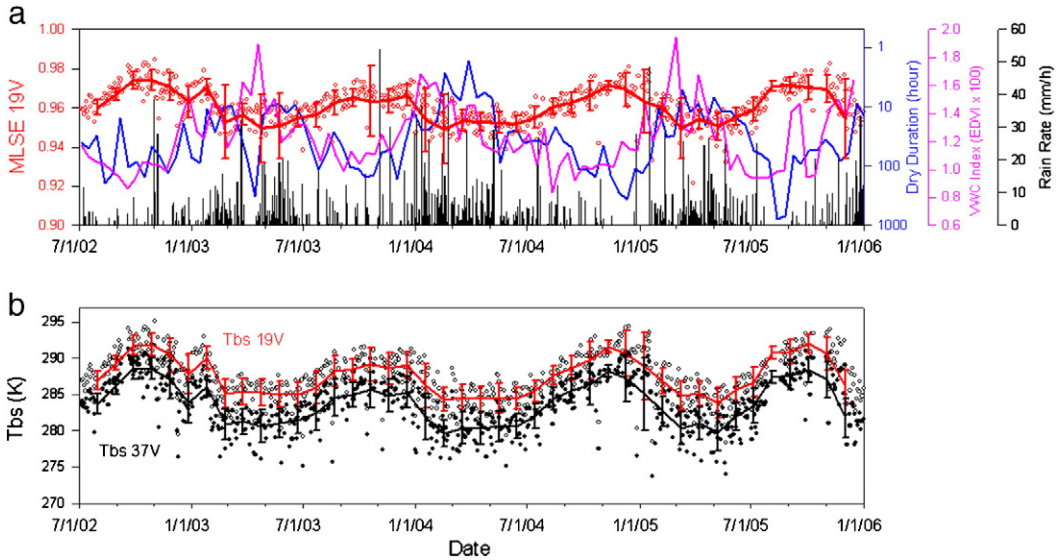


**Fig. 3.** Time series of (a) MLSE at 19 GHz (V polarization), dry duration, EDVI the vegetation water content index and rain rate; (b) 19 and 37 GHz brightness temperatures (V polarization) at Km67 site.

microwave land surface emissivity MLSE ($\varepsilon$) at the top of the canopy as:

$$\varepsilon = \varepsilon_s e^{-\tau/\mu} + \left(1-e^{-\tau/\mu}\right)(1-\omega). \quad (3)$$

Because vegetation and soil are a coupled system, MLSE is complicatedly related to SM, as shown in Eq. (4):

$$\frac{\partial \varepsilon}{\partial \mathrm{SM}} = e^{-\tau/\mu}\frac{\partial \varepsilon_s}{\partial \mathrm{SM}} - \frac{1}{\mu}[\varepsilon_s-(1-\omega)]e^{-\tau/\mu}\frac{\partial \tau}{\partial \mathrm{SM}} - \left(1-e^{-\tau/\mu}\right)\frac{\partial \omega}{\partial \mathrm{SM}}. \quad (4)$$

If assuming vegetation properties are independent or weakly dependent on SM, the first term in Eq. (4) prevails. As the soil emissivity decreases with SM, i.e. $\partial\varepsilon_s/\partial SM<0$, the sensitivity of MLSE to SM is also negative with an attenuation effect from the vegetation. Fig. 4 shows that both MLSE and Tbs at all three frequencies are negatively correlated with the in-situ soil moisture and these correlations are statistically significant. It is consistent with theoretical analysis and previous studies (Lin & Minnis, 2000; Prigent et al., 2005; and others). Relatively, the microwave properties at 19 and 37 GHz have a similar sensitivity to the soil moisture and are stronger than those at 24 GHz, probably due to the lesser influence of water vapor.

In the dense vegetation regime, such as Amazon rainforest, the soil moisture signal should be substantially attenuated by the vegetation, resulting in decoupling between MLSE and SM. The observed sensitivity of MLSE to soil moisture, however, could stem from 1) the inherent linkage between soil moisture and vegetation water content, and 2) the contribution from the soil moisture signals of agriculture patches and uncovered bare soil spots (roads) with the footprint of AMSR-E.

### 3.2. Vegetation

The noisiness in Fig. 4 and the complexity of Eq. (4) manifest the facts that 1) vegetation also plays a key role in determining MLSE at the top of the canopy. As pointed out by Jackson and Schmugge (1991), the vegetation optical depth at microwave wavelengths has a semi-empirical relation with VWC, i.e., $\tau = b \cdot \mathrm{VWC}$, in which coefficient $b$ varies systematically with both wavelength and canopy structure. To investigate the impact of VWC on MLSE, we explicitly take the derivative of VWC in Eq. (3). Hence, the sensitivity of MLSE to vegetation is:

$$\frac{\partial \varepsilon}{\partial \mathrm{VWC}} = -\frac{e^{-\tau/\mu}}{b\mu}[\varepsilon_s-(1-\omega)] - \left(1-e^{-\tau/\mu}\right)\frac{\partial \omega}{\partial \mathrm{VWC}}. \quad (5)$$

Although Lin et al. (2008) found the effective single scattering albedo of vegetation is sensitivity to its VWC, the direct measurement of ω is not available in this study. We just ignore the term associated with $\partial\omega/\partial$VWC for simplicity. A more comprehensive discussion about this effect requires more detailed radiation transfer model taking into account of both the surface and canopy scattering. The sensitivity of MLSE to VWC could be either positive or negative, depending on the partition between vegetation $(1-\omega)$ and soil emission ($e_s$) characteristics. Fig. 5 clearly shows such complicated MLSE–VWC (EDVI) relationships at all three frequencies: i.e., MLSEs as well as Tbs increase when VWC (EDVI) is small and then decrease with VWC when VWC is large. This non-monotonic dependence of MLSE on VWC is consistent with the theoretic calculation of Min and Lin (2006a). Specifically, when EDVI is smaller than 0.007 in this case, both Tbs and associated MLSE increase with EDVI; when the EDVI is

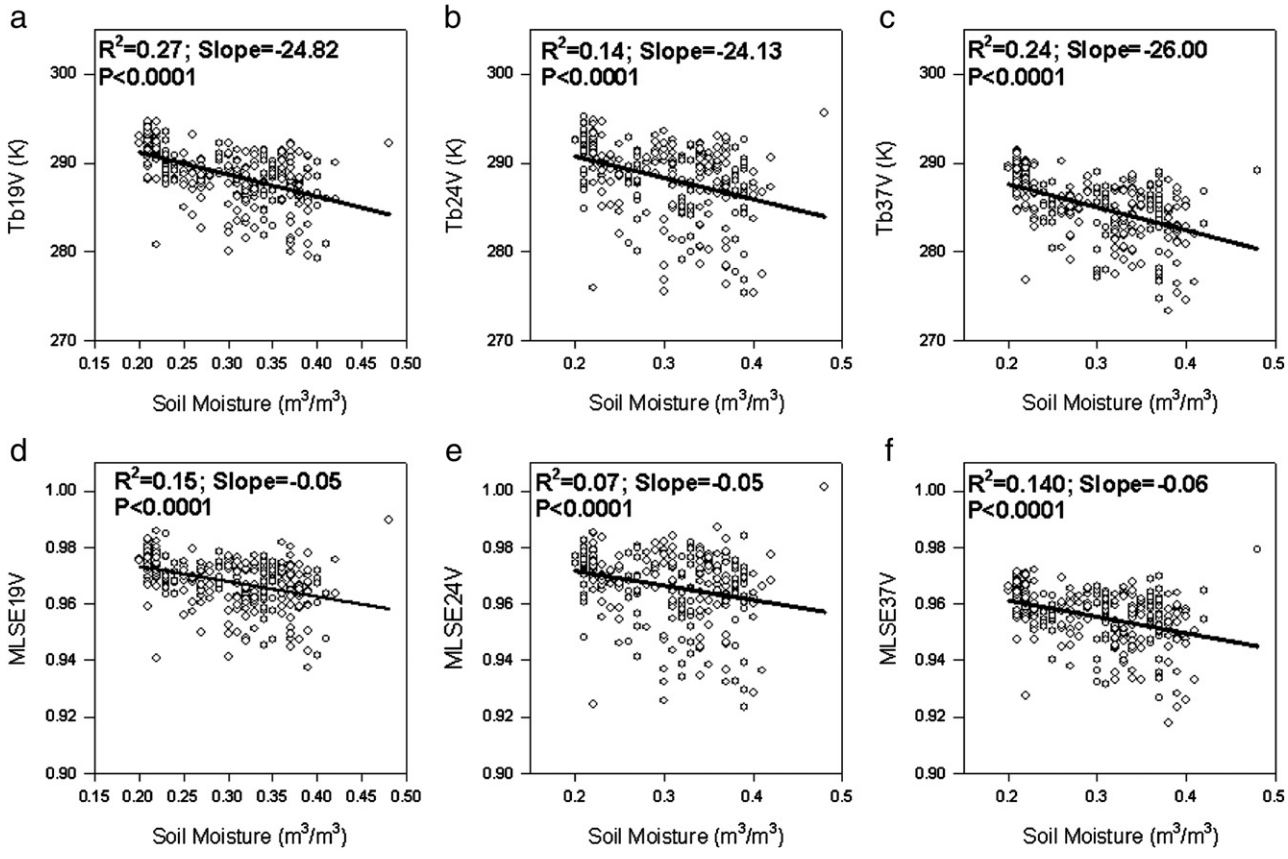


**Fig. 4.** The scatter plots of Tbs and MLSEs at (a,d) 19 GHz; (b,e) 24 GHz and (c,f) 37 GHz against soil moisture at the Km83 site.

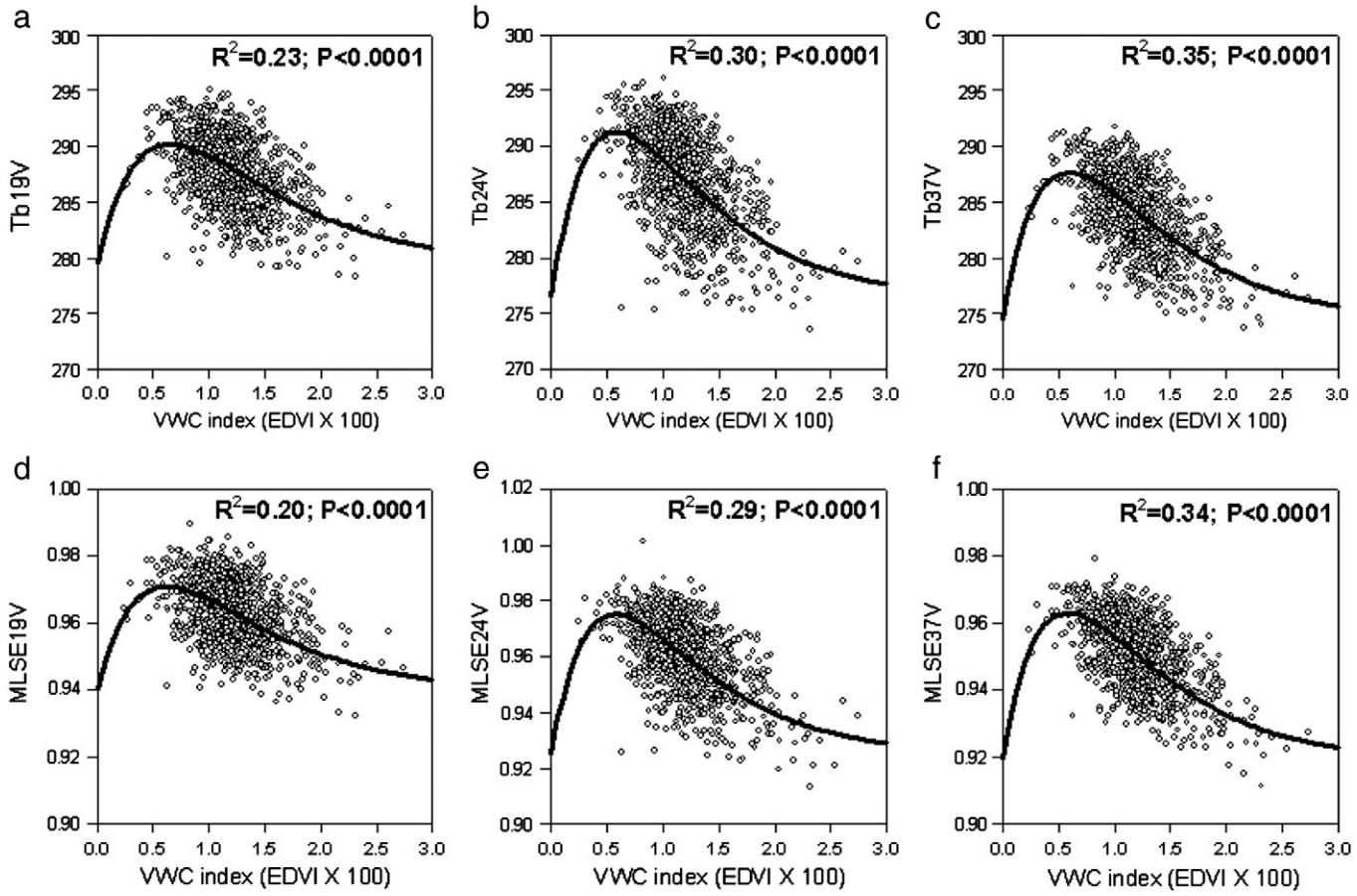


**Fig. 5.** The scatter plots of Tbs and MLSEs at (a,d) 19 GHz; (b,e) 24 GHz and (c,f) 37 GHz against EDVI the index of vegetation water content at both the Km83 and Km67 sites. The overlapped fitting curves are in the linear–exponential function of $y = y_0 + axEXP(-bx)$ ($y_0 > 0$; $a > 0$; $b > 0$).

larger than ~0.007, both Tbs and MLSEs decrease with EDVI. The dependence of Tbs and MLSE on EDVI can be fitted with a linear–exponential function:

$$\mathrm{Tb(MLSE)} = \mathrm{Tb_0(MLSE_0)} + a\mathrm{EDVI}\exp(-b\mathrm{EDVI}). \quad (6)$$

The correlation coefficients and associated parameters of in Eq. (6) are listed in Table 1. Basically, with a high SM and consequently a low soil emissivity, MLSE increases with VWC for low VWC, due to the scattering and emission effects of the vegetation. However, when VWC is high enough, the strong absorption of the vegetation attenuates the soil emission, resulting in MLSE dominated by the vegetation emissivity that decreases with VWC.

Our finding differs from the monotonic positive correlation between MLSE and vegetation reported by some previous studies (Aires et al., 2005; Morland et al., 2000, 2001; Prigent et al., 2005), in which the Normalized Difference Vegetation Index (NDVI) is used to represent the vegetation. At small VWC, they are consistent with each other. As the Amazon rainforest is in dense vegetation regime, our results provide new insights about the relationship for a larger range of VWC.

**Table 1**
Parameters in the linear–exponential fitting of Tb and MLSE to EDVI.

| | Tb (K) | | | MLSE | | |
|---|---|---|---|---|---|---|
| | 19 GHz | 24 GHz | 37 GHz | 19 GHz | 24 GHz | 37 GHz |
| $y_0$ | 279.57 | 276.52 | 274.53 | 0.940 | 0.925 | 0.919 |
| $a$ | 4389.34 | 6918.92 | 5951.84 | 13.563 | 23.78 | 20.30 |
| $b$ | 152.36 | 172.41 | 166.98 | 161.317 | 175.260 | 170.838 |
| $R^2$ | 0.23 | 0.30 | 0.35 | 0.20 | 0.29 | 0.34 |

### 3.3. The precipitation

Precipitation and associated clouds play a pivotal role in the soil–vegetation–atmosphere interactions and modulate the soil moisture and vegetation water content. For physically-based overland rainfall retrievals, both rainy pixel classification and rain rate quantification require the knowledge of Tb and MLSE under cloudy and even rainy conditions. However, the direct retrieval of Tb and MLSE under rainy conditions from satellite passive microwave measurements is not easy, if not impossible, due to the strong emission, scattering, and absorption effects from precipitating hydrometeors. A feasible approach is to extrapolate MLSE from the non-rainy or "near rain" conditions to the rainy condition. The impacts of SM and VWC on Tb and MLSE discussed in the previous subsections provide the fundamental understanding to establish such a linkage. Specifically, we will focus on the behavior of MLSE in terms of dry duration (DD), since DD equals zero when it rains.

To understand the dynamics of Tb and MLSE after precipitation, we first investigate the responses of soil moisture and vegetation water content to precipitation. As shown in Fig. 6a for three randomly selected rain events, SM firstly increased gradually in response to precipitation, peaked a few hours later after the start of rain due to interception and infiltration processes, and then decreased gradually as a result of evapotranspiration. The time for SM to reach its maximum and the magnitude of the maximum strongly depend on the rain duration, the rain rate, the canopy structures, and the soil type. It should

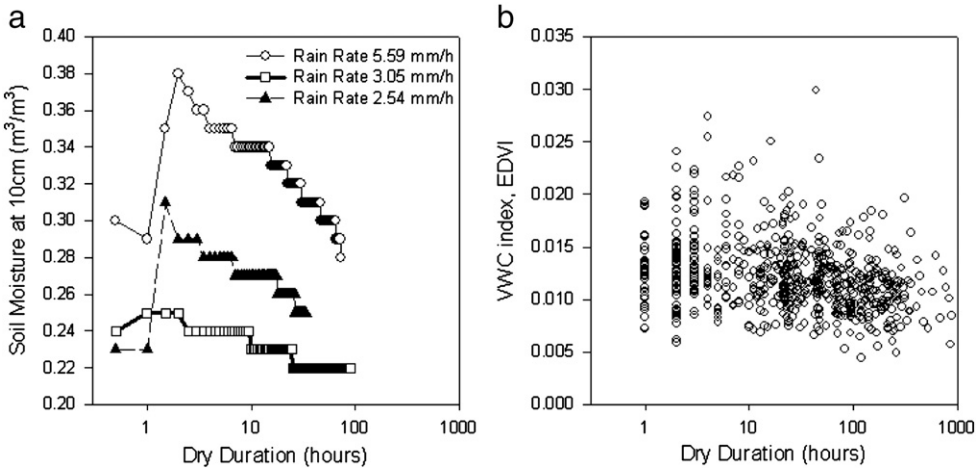


**Fig. 6.** (a) The observed response of SM to precipitation in three selected isolated rain events in Km83 site; (b) The scatter plot of observed EDVI the index of VWC against dry duration using all proper samples in Km83 and Km67 sites.

be noticed that the near-surface SM may be peak earlier than the SM at 10 cm measured here, due to infiltration processes.

There was no direct measurement of VWC and interception water at the site. Instead, the field measurements of the diurnal xylem diameter change at different heights in a 37-year-old Scots pine at Hyytiälä, southern Finland showed the swelling of xylem associated precipitation, as a result of changes in transpiration and soil water tension, suggesting an increase of VWC after precipitation (Perämäki et al., 2001; Sevanto et al., 2005a, 2005b). It also provides the evidence of inherent coupling between soil moisture and VWC. Also, as estimated by Czikowsky and Fitzjarrald (2009), the mean interception was about 10% at the Km67 site, depending on the rain duration and the rain rate. The mean intercepted water per rain event was about 0.1 mm/m$^2$ or 0.1 kg/m$^2$, which is one order magnitude smaller than VWC in the canopy crown leaves (not including branches and twigs) of 1.5–3.5 kg/m$^2$. The intercepted water (both on the leaves and over the surface) in general

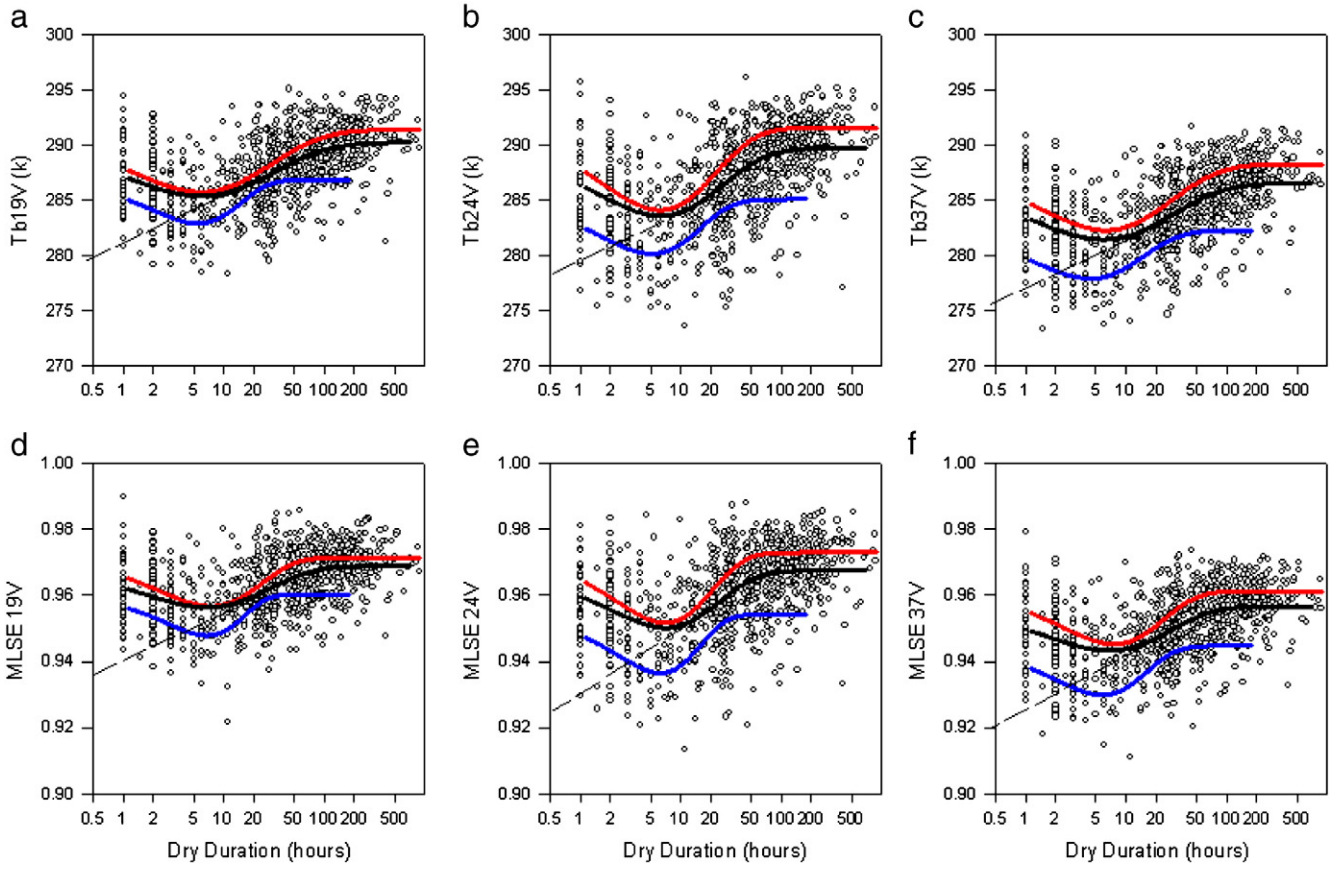


**Fig. 7.** The scatter plots of Tbs and MLSEs at (a,d) 19 GHz; (b,e) 24 GHz and (c,f) 37 GHz against dry duration (DD, hours, in logarithm) at both the Km83 and Km67 sites. The overlapped fitting curves are in the function of $Y = Y_0 - AxEXP(-Bx^C)$ ($Y_0 > 0$; $A > 0$; $B > 0$; $C > 0$, see Table 2 for details). The different colors for the fitting curves stand for: Red for samples with EDVI 0–0.0005; Black for samples with EDVI 0.0005–0.015; Blue for samples with EDVI > 0.015. The dashed reference lines stand for simple linear extrapolations of the curve from large DD to DD zero (i.e. rainy condition).

evaporated within 4 h after the first rain tip (Czikowsky & Fitzjarrald, 2009). Although EDVI cannot be retrieved during rain events, the combined VWC and intercepted water as indicated by EDVI, shown in Fig. 6b, increased with DD and started to decrease gradually after certain time point. Clearly, the canopy experiences dynamical changes in soil and vegetation within several hours after precipitation.

The changes in MLSE and Tbs after precipitation as a function of DD are shown in Fig. 7, exhibiting two distinct tendencies for all frequencies. It took about 4 h on average to reach the minimum values of MLSE and Tbs. With the persistence of dry conditions after that time, MLSE and Tbs gradually increase.

Fig. 8 illustrates the conceptual changes of SM, VWC, and interception water, and MLSE in response to precipitation. As found in the real observation (Fig. 6) after the start of rain, soil moisture, VWC and interception water all increase and reach their maximum values with different transit times. The SM reaches its peak earlier than the VWC because it takes time for surface water to reach the root zone via infiltration and additional time to uptake water from their root zone to leaves. The peak time of the interception water highly depends on the rain intensity, rain duration and the vegetation structure. There is no direct observation on how the interception water impacts on MLSEs and Tbs. We suspect that its impacts are overwhelmed by vegetation due to its relatively small water mass compared to VWC. Due to the correlations of MLSE (and Tbs) and SM and VWC, the increase of SM and VWC in the first several hours after rain leads to the decreases of MLSE and Tbs, as observed in Fig. 7 when DD<4 h. This is the time duration required for precipitating water to settle within the canopy, resulting in an equilibrium time point at which the vegetation–soil system hold the largest amount of moisture and has the minimum values of MLSE and Tbs. The four-hour transit time is consistent with the time of interception evaporation found by Czikowsky and Fitzjarrald (2009). As the evapotranspiration process dried up the canopy, MLSE and Tbs gradually increased after the equilibrium time point.

Precipitation induced changes in MLSE and the transit time to its minimum are strongly dependent on antecedent soil moisture and vegetation conditions, canopy structures (root, trunk, branch, leave), and precipitation characteristics (rain duration, rain rate). The transit time will be short for short and sparse vegetation, and nearly none for bare soil. Most of the current estimations of MLSE are obtained under clear-sky conditions, and the clear-sky condition is usually a few hours after precipitation events. As shown in Figs. 7 and 8, a simple linear extrapolation from the clear-sky MLSE value to the rainy MLSE value (DD = 0) would result in an underestimation of $\Delta\varepsilon$. $\Delta\varepsilon$ can be as high as ~0.03–0.04 at 19 and 37 GHz, shown in Fig. 7, respectively. Consequently, the associated errors in Tbs will be about 10 K. On the other hand, simply using the clear sky MLSE values without extrapolation would result in overestimation of $\Delta\varepsilon'$.

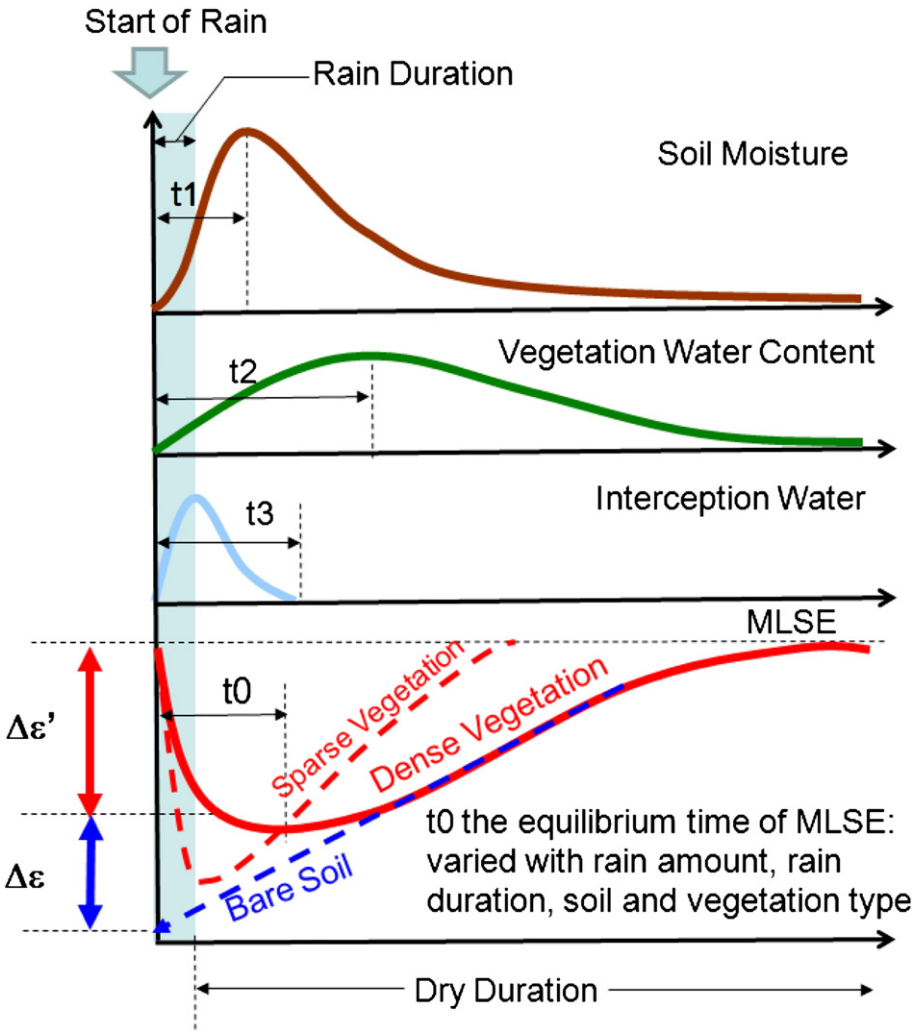


**Fig. 8.** Conceptual plot describing the responses of soil moisture, vegetation water content, interception water and the associate microwave land surface emissivity to the precipitation.

**Table 2**
Parameters in the linear–exponential fitting of Tb and MLSE to dry duration (in three different EDVI ranges).

| | | Tb (K) | | | MLSE | | |
|---|---|---|---|---|---|---|---|
| | | 19 GHz | 24 GHz | 37 GHz | 19 GHz | 24 GHz | 37 GHz |
| EDVI<0.0005 | $Y_0$ | 291.39 | 291.56 | 288.27 | 0.972 | 0.973 | 0.961 |
| | $A$ | 14.15 | 7.18 | 10.53 | 0.008 | 0.011 | 0.009 |
| | $B$ | 1.40 | 0.64 | 1.12 | 0.356 | 0.286 | 0.340 |
| | $C$ | 0.37 | 0.56 | 0.42 | 0.693 | 0.775 | 0.704 |
| | $R^2$ | 0.31 | 0.37 | 0.33 | 0.23 | 0.30 | 0.25 |
| EDVI 0.0005–0.015 | $Y_0$ | 290.23 | 289.72 | 286.54 | 0.969 | 0.967 | 0.957 |
| | $A$ | 14.43 | 8.26 | 12.32 | 0.016 | 0.013 | 0.016 |
| | $B$ | 1.54 | 0.90 | 1.37 | 0.882 | 0.504 | 0.827 |
| | $C$ | 0.35 | 0.47 | 0.37 | 0.465 | 0.607 | 0.482 |
| | $R^2$ | 0.25 | 0.25 | 0.25 | 0.20 | 0.21 | 0.21 |
| EDVI>0.015 | $Y_0$ | 286.86 | 285.08 | 282.26 | 0.960 | 0.954 | 0.945 |
| | $A$ | 2.13 | 3.64 | 4.69 | 0.004 | 0.007 | 0.008 |
| | $B$ | 0.22 | 0.39 | 0.61 | 0.089 | 0.140 | 0.240 |
| | $C$ | 0.92 | 0.75 | 0.64 | 1.179 | 1.046 | 0.882 |
| | $R^2$ | 0.18 | 0.16 | 0.18 | 0.19 | 0.19 | 0.20 |

The joint soil–vegetation effect of precipitation can be parameterized as a linear–exponential function of dry duration:

$$\mathrm{Tb(MLSE)} = \mathrm{Tb_0(MLSE_0)} + \mathrm{A{\cdot}DD}\exp\left(-\mathrm{B{\cdot}DD^C}\right). \quad (7)$$

The linear–exponential relationship can be further parameterized for different ranges of EDVI, with better correlation coefficients (the fitting coefficients are listed in Table 2). The correlation coefficients are statistically significant and decrease with VWC index or EDVI. It is worth noting that the fitting coefficients are a function of soil properties and canopy structures. Overall, Tb and MLSE vary with dry duration (DD) linear-exponentially, consistent with our conceptual model. The conceptual model, as well as Eq. (7), provides a way to understand the impacts of precipitation on MLSE.

## 4. Discussion and conclusion

To understand the dynamics of the microwave land surface properties, including Tbs and MLSE, at different time scales and to parameterize those under rainy conditions, require synergized products of both satellite retrieved MLSE and associated environmental parameters. This study is built upon our all-weather (non-rain) MLSE retrieval algorithm to obtain satellite MLSE retrievals close to precipitation events under cloudy conditions (Min & Lin, 2006a; Min et al., 2010). We integrated satellite MLSE retrievals with surface and other meteorological measurements at two Amazon forest sites to study the impacts of soil moisture, vegetation water content, and precipitation on MLSE and Tbs.

Although Amazon dense rainforest is the most stable vegetation regime, there are significant seasonal variations in both MLSE and Tbs, with amplitudes of about 0.025 and 7.0 K, respectively. At the seasonal scale, MLSE and Tbs are anti-correlated with VWC indicated by EDVI, with modulation of seasonal soil moisture variation. The day-to-day variation of MLSE and Tbs is larger in the wet seasons than in the dry seasons, although the mean MLSE and Tbs are lower in the wet seasons than in the dry seasons.

For the dense vegetation like the Amazon tropical rainforests we studied, microwave signals are supposed to be insensitive to soil moisture due to strong vegetation absorption. However, there is an apparent relationship between MSLE (and Tbs) and soil moisture found in this study and the anti-correlation is statistically significant. Either the soil moisture signal has not been fully blocked by the forest or the soil moisture signal is indirectly observable through VWC due to the inherent coupling of VWC with soil moisture.

As the forests at our study sites are in a dense vegetation regime, the impact of VWC on MSLE (and Tbs) is no long a linear relationship as reported by many previous researches (Morland et al., 2000, 2001; Norouzi et al., 2001; Prigent et al., 2005; Ruston & Vonder Haar, 2004). At relatively low VWC values, MLSE does increase with VWC, consistent with previous findings. However, when VWC is higher than a threshold, MLSE decreasing with VWC prevails. The anti-correlation between MLSE and VWC is clearly evident at seasonal scales. Our theoretic analysis further suggested that the threshold or critical point is not simply dependent on VWC but on the balance between soil emissivity and vegetation emissivity (or 1 — single scattering albedo). The latter is a function of vegetation structure and optical properties.

Precipitation directly changes soil moisture and interception water, and indirectly modulates vegetation water content. The precipitation induced changes in MLSE and Tbs exhibit two distinct regimes: a decreasing tendency in the first few hours and then an increasing tendency for the persisting dry period. Based on the observed responses of soil moisture, vegetation water content, and intercepted water changes to adjacent rain events, we proposed a simple conceptual model to explain the dynamics of MLSE in response to precipitation. Part of the precipitation water is intercepted by the vegetation and the rest is infiltrated into the soil to enhance soil moisture at the upper humus layer and slowly into the deep root zone. The infiltration and later transpiration processes result in soil moisture reaching a maximum after certain transit time. In the meantime, the swelling of xylem due to changes in transpiration and soil water tension leads to increases of VWC. The increases in both SM and VWC in concert result in a decrease in Tbs and MLSE before the precipitating water settle in the vegetation–soil system. After precipitation and in the daytime (our study only focused on daytime overpasses), the evaporation dries out the water both on the leaves, over the land surface and within the canopy in a few hours (less than 4 h according to Czikowsky & Fitzjarrald, 2009). Sequentially after the intercepted water evaporated and the soil–vegetation system reached its equilibrium, the evapotranspiration reduces both soil moisture and VWC when the dry duration persists, resulting MLSE increases. Precipitation induced changes in MLSE are strongly dependent on antecedent soil moisture and vegetation conditions, canopy structures (root, trunk, branch, leave), and precipitation characteristics (rain duration, rain rate). The conceptual model illustrates inherent responses of soil and vegetation to precipitation.

Our goal is to extrapolate the MLSE from non-rainy or “near rain” conditions to that under rainy condition. A simple assumption of MLSE always decreasing with the dry duration after rains will introduce substantial errors in the MLSE extrapolation. Our empirical fitting provides a more accurate means for such an extrapolation. As discussed previously, without a proper extrapolation, substantial errors may exist in the rainy MSLE estimations, up to 0.03–0.04 at 19 and 37 GHz, respectively. Certainly, our observed behaviors of SM, VWC, intercepted water, and MSLE as a function of dry duration differ from regime to regime. It warrants further and extensive investigation at various climate and vegetation regimes.

## References


Aires, F., Prigent, C., & Rossow, W. B. (2005). Sensitivity of satellite microwave and infrared observations to soil moisture at a global scale: 2. Global statistical relationships. *Journal of Geophysical Research*, *110*, D11103. http://dx.doi.org/10.1029/2004JD005094.

Asrar, G. E., Fuchs, M., Kanemasu, E. T., & Hatfield, J. L. (1984). Estimating absorbed photosynthetic radiation and leaf area index from spectral reflectance in wheat. *Agronomy Journal*, *76*, 300–306.

Czikowsky, M. J., & Fitzjarrald, D. R. (2009). Detecting rainfall interception in an Amazonian rain forest with eddy flux measurements. *Journal of Hydrology*, *377*, 92–105.

Ferraro, R., Peters-Lidard, C., Hernandez, C., Turk, F. J., Aires, F., Prigent, C., et al. (2013). An evaluation of microwave land surface emissivities over the continental United States to benefit GPM-era precipitation algorithms. *IEEE Transactions on Geosciences and Remote Sensing*, *51*, 378.

Granger, R. J. (2000). Satellite-derived estimates of evapotranspiration in the Gediz basin. *Journal of Hydrometeorology*, *229*, 70–76.

Grody, N. C. (1991). Classification of snow cover and precipitation using the Special Sensor Microwave/Imager (SSM/I). *Journal of Geophysical Research*, *96*, 7423–7435.

Gutman, G. (1999). On the use of long-term global data of land reflectances and vegetation indices derived from the advanced very high resolution radiometer. *Journal of Geophysical Research*, *104*, 6241–6255.

Hutyra, L. R., Munger, J. W., Saleska, S. R., Gottlieb, E., Daube, B. C., Dunn, A. L., et al. (2007). Seasonal controls on the exchange of carbon and water in an Amazonian rain forest. *Journal of Geophysical Research*, *112*, G03008. http://dx.doi.org/10.1029/2006JG000365.

Jackson, T. J., & Schmugge, T. J. (1991). Vegetation effects on the microwave emission of soils. *Remote Sensing of Environment*, *36*, 203–212.

Jiménez, C., Prigent, C., Catherinot, J., Rossow, W., Liang, P., & Moncet, J. -L. (2012). A comparison of ISCCP land surface temperature with other satellite and in situ observations. *Journal of Geophysical Research*, *117*, D08111. http://dx.doi.org/10.1029/2011JD017058.

Li, R., Min, Q., & Lin, B. (2009). Estimation of evapotranspiration in a mid-latitude forest using the microwave emissivity difference vegetation index (EDVI). *Remote Sensing of Environment*, *113*, 2011–2018.

Lin, B., & Minnis, P. (2000). Temporal variations of land surface microwave emissivities over the ARM Southern Great Plains Site. *Journal of Applied Meteorology*, *39*, 1103–1116.

Lin, B., Minnis, P., Fan, A., Curry, J., & Gerber, H. (2001). Comparison of cloud liquid water paths derived from in situ and microwave radiometer data taken during the SHEBA/FIREACE. *Geophysical Research Letters*, *28*, 975–978.

Lin, B., Wielicki, B., Minnis, P., & Rossow, W. B. (1998). Estimation of water cloud properties from satellite microwave, infrared, and visible measurements in oceanic environments. I: Microwave brightness temperature simulations. *Journal of Geophysical Research*, *103*, 3873–3886.

Lin, B., Sun, W., Min, Q., & Hu, Y. (2008). Numerical studies of scattering properties of leaves and leaf moisture influences on the scattering at microwave wavelengths. *IEEE Transactions on Geosciences and Remote Sensing*, *46*, 353–360.

Liu, G., Curry, J. A., & Weadon, M. (1994). Atmospheric water balance in typhoon Nina as determined from SSM/I satellite. *Meteorology and Atmospheric Physics*, *54*, 141–156.

Miller, S., Goulden, M., & Rocha, H. R. da. (2009). LBA-ECO CD-04 Meteorological and Flux Data, km 83 Tower Site, Tapajos National Forest. Data set. Available on-line [http://daac.ornl.gov] from Oak Ridge National Laboratory Distributed Active Archive Center, Oak Ridge, Tennessee, U.S.A. http://dx.doi.org/10.3334/ORNLDAAC/946.

Min, Q. (2005). Impacts of aerosols and clouds on $CO_2$ uptake over Harvard Forest. *Journal of Geophysical Research*, *110*(D6), D06203. http://dx.doi.org/10.1029/2004JD004858.

Min, Q., & Lin, B. (2006a). Remote sensing of evapotranspiration and carbon uptake at Harvard Forest. *Remote Sensing of Environment*, *100*, 379–387.

Min, Q., & Lin, B. (2006b). Determination of spring onset and growing season duration using satellite measurements. *Remote Sensing of Environment*, *104*, 96–102.

Min, Q., Lin, B., & Li, R. (2010). Remote sensing vegetation hydrological states using passive microwave measurements. *IEEE Journal of Selected Topics in Applied Earth Observation and Remote Sensing*, *3*(1), 124–131. http://dx.doi.org/10.1109/JSTARS.2009.2032557.

Morland, J. C., Grimes, D. I. F., Dugdale, G., & Hewison, T. J. (2000). The estimation of land surface emissivities at 24 GHz to 157 GHz using remotely sensed aircraft data. *Remote Sensing of Environment*, *73*(3), 323–336.

Morland, J. C., Grimes, D. I. F., & Hewison, T. J. (2001). Satellite observations of the microwave emissivity of a semi-arid land surface. *Remote Sensing of Environment*, *77*(2), 149–164.

Myneni, R. B., Hall, F. B., Sellers, P. J., & Marshak, A. L. (1995). The interpretation of spectral vegetation indices. *IEEE Transactions on Geoscience and Remote Sensing*, *33*, 481–486.

Njoku, E. G. (1999). "AMSR land surface parameters", ATBD 3.0, Jet Propulsion Lab. http://eospso.gsfc.nasa.gov/ftp_ATBD/REVIEW/AMSR/atbd-amsr-land.pdf

Norouzi, H., Temimi, M., Rossow, W. B., Pearl, C., Azarderakhsh, M., & Khanbilvardi, R. (2001). The sensitivity of land emissivity estimates from AMSR-E at C and X bands to surface properties. *Hydrology and Earth System Sciences*, *15*, 3577–3589. http://dx.doi.org/10.5194/hess-15-3577-2011.

Perämäki, M., Nikinmaa, E., Sevanto, S., Ilvesniemi, H., Siivola, E., Hari, P., et al. (2001). Tree stem diameter variation and transpiration in Scots pine; An analysis using dynamic sap flow model. *Tree Physiology*, *21*, 889–897.

Prigent, C., Aires, F., Rossow, W. B., & Robock, A. (2005). Sensitivity of satellite microwave and infrared observations to soil moisture at a global scale: Relationship of satellite observations to in situ soil moisture measurements. *Journal of Geophysical Research*, *110*, D07110. http://dx.doi.org/10.1029/2004JD005087.

Ruston, B. C., & Vonder Haar, T. H. (2004). Characterization of summertime microwave emissivities from the Special Sensor Microwave Imager over the conterminous United States. *Journal of Geophysical Research*, *109*, D19103.1–D19103.13.

Saleska, S. R., Miller, S. D., Matross, D. M., Goulden, M. L., Wofsy, S. C., da Rocha, H., et al. (2003). Carbon fluxes in old-growth Amazonian rainforest: Seasonality and disturbance-induced net carbon loss. *Science*, *302*, 1554–1557.

Sellers, P. J. (1985). Canopy reflectance, photosynthesis, and transpiration. *International Journal of Remote Sensing*, *6*, 1335–1372.

Sevanto, S., Hölttä, T., Hirsikko, A., Vesala, T., & Nikinmaa, E. (2005a). Determination of thermal expansion of green wood and the accuracy of tree stem diameter variation measurements. *Boreal Environment Research*, *10*, 437–445.

Sevanto, S., Hölttä, T., Markkanen, T., Perämäki, M., Nikinmaa, E., & Vesala, T. (2005b). Relationships between diurnal xylem diameter variation and environmental factors in Scots pine. *Boreal Environment Research*, *10*, 447–458.

Spencer, R. W., Goodman, M. H., & Hood, E. R. (1989). Precipitation retrieval over land and ocean with the SSM/I: Identification and characteristics of the scattering signal. *Journal of Atmospheric and Oceanic Technology*, *6*, 254–273.

Ulaby, F. T., Moore, R. K., & Fung, A. K. (1986). *Microwave remote sensing active and passive. From theory to applications*, *vol. III*, London, U.K.: Artech House.

Yang, H., & Weng, F. (2011). Error sources in remote sensing of microwave land surface emissivity. *IEEE Transactions on Geoscience and Remote Sensing*, *49*(9), 3437–3442. http://dx.doi.org/10.1109/TGRS.2011.2125794.

Zheng, W., Wei, H., Wang, Z., Zeng, X., Meng, J., Mitchell, M., et al. (2012). Improvement of daytime land surface skin temperature over arid regions in the NCEP GFS model and its impact on satellite data assimilation. *Journal of Geophysical Research*, *117*, D06117. http://dx.doi.org/10.1029/2011JD015901.